John Carroll University
Carroll Collected

2019 Faculty Bibliography | Faculty Bibliographies Community Homepage

2019

Genetic Analysis of a Cryptic Contact Zone between Mitochondrial Clades of the Eastern Red-Backed Salamander, Plethodon cinereus

Brian P. Waldron
Ohio Center for Ecology and Evolutionary Studies

Shawn R. Kuchta
Ohio Center for Ecology and Evolutionary Studies

Maggie M. Hantak
Ohio Center for Ecology and Evolutionary Studies

Cari-Ann M. Hickerson
John Carroll University

Carl D. Anthony
John Carroll University, canthony@jcu.edu

Follow this and additional works at: https://collected.jcu.edu/fac_bib_2019

Part of the Biology Commons, and the Ecology and Evolutionary Biology Commons

Recommended Citation

Waldron, Brian P.; Kuchta, Shawn R.; Hantak, Maggie M.; Hickerson, Cari-Ann M.; and Anthony, Carl D., "Genetic Analysis of a Cryptic Contact Zone between Mitochondrial Clades of the Eastern Red-Backed Salamander, Plethodon cinereus" (2019). *2019 Faculty Bibliography*. 29.
https://collected.jcu.edu/fac_bib_2019/29

This Article is brought to you for free and open access by the Faculty Bibliographies Community Homepage at Carroll Collected. It has been accepted for inclusion in 2019 Faculty Bibliography by an authorized administrator of Carroll Collected. For more information, please contact connell@jcu.edu.

Genetic Analysis of a Cryptic Contact Zone between Mitochondrial Clades of the Eastern Red-Backed Salamander, *Plethodon cinereus*

Abstract.—When evolutionarily divergent lineages adjoin their geographic ranges after a period of isolation, myriad outcomes can occur, from population anastomosis to the evolution of reproductive isolation by way of reinforcement. Hybrid zones represent natural experiments that may indicate whether lineages will maintain their evolutionary independence. Here, we report on a hybrid zone in the Eastern Red-Backed Salamander, *Plethodon cinereus*, a highly abundant and wide-ranging terrestrial salamander found in the northeastern United States and in southeastern Canada. An earlier study identified six distinct mitochondrial clades across the range of *P. cinereus*. Populations of two of these clades were as close as 9.6 km apart in Lorain County, Ohio, USA. To investigate the nature of this contact zone, we sampled 316 individuals from 16 sites along a 53-km transect, and analyzed 10 microsatellite loci and one mitochondrial locus. We found a clinal transition for mtDNA haplotypes. In contrast, most studies of terrestrial plethodontid salamanders commonly exhibit sharp boundaries between mtDNA clades. Microsatellite markers, however, revealed little differentiation and weak population structure, suggesting the nuclear cline, if it exists, lies outside of our sampling region. Explanations for the discordance between the mitochondrial DNA and our microsatellite data include lineage sorting, male-biased dispersal, or historical introgression of mtDNA, among other possibilities. We compare our results with other studies of introgression in terrestrial salamanders, and discuss the causes of mitonuclear discordance.

Secondary contact zones, where formerly geographically isolated populations recontact, provide ideal natural systems for evolutionary biologists to study the factors that influence the genetic independence of evolutionary lineages (Harrison, 1993). Analyzing geographic transitions in morphological traits and genetic markers between interacting populations at points of secondary contact allows for inference of the strength and mode of selection operating on traits, and estimation of the degree of reproductive isolation (Barton and Hewitt, 1989). Although hybridization (referring to interbreeding or backcrossing between genetically distinct populations) can often be diagnosed using anatomical characters (e.g., Kuchta, 2007; Gay et al., 2008; Devitt et al., 2011), some contact zones involve parent populations that are difficult to distinguish morphologically (e.g., Highton, 1999; Martínez-Solano et al., 2007). Genetic markers are particularly useful for studying cryptic contact zones because they can reveal patterns of genetic structure and gene flow between morphologically similar, yet genetically differentiated, populations.

In this paper, we report on a study of a cryptic contact zone in the Eastern Red-Backed Salamander, *Plethodon cinereus*. For many eastern North American herpetofauna, ice sheets and climate change have limited northern ranges during the Last Glacial Maximum (LGM) about 22,000–18,000 years before present (Dyke, 2004). Climatic oscillations of the Pleistocene and eventual deglaciation led to dynamic phylogeographic patterns, often with divergence in multiple refugia, followed by secondary contact (e.g., *Ambystoma maculatum*, Zamudio and Savage, 2003; *Rana sylvatica*, Lee-Yaw et al., 2008; *Plethodon serratus*, Newman and Austin, 2015; Thesing et al., 2016; *Eurycea lucifuga*, Edgington et al., 2016). In some amphibian species, previously glaciated northern regions comprise a large portion of the species range, providing natural systems to study range expansion and the secondary contact of multiple colonizing lineages.

Plethodon cinereus is one of the most abundant terrestrial vertebrates in eastern North America (Burton and Likens, 1975), and ranges from North Carolina, USA, to southern Canada. Much of the current range of *P. cinereus* overlaps with regions that were covered by ice sheets during the LGM. Little allozyme genetic variation exists among widely distributed populations across the previously glaciated parts of the range, despite considerable genetic structure among populations to the south (Highton and Webster, 1976; Hass, 1985). This pattern suggests rapid northern expansion following deglaciation, with the source populations along the Atlantic coast (Hass, 1985). In addition, a study of population structure in *P. cinereus* in northern Indiana using microsatellites also found a lack of both population structure and isolation-by-distance, which also suggests rapid post-Pleistocene range expansion (Jordan et al., 2009).

More recently, phylogeographic analyses with mtDNA recovered six distinct mtDNA clades, with coalescence times estimated at 1.42 million years (95% highest posterior density [HPD]: 1.12–2.36 million years ago [Ma]; Radomski, 2017), although with processes such as incomplete lineage sorting in single-locus estimates, the actual divergence dates may be more recent (Edwards, 2009). Three of these clades inhabit the postglacial landscape, all of which are found in northern Ohio, USA. Two of these clades, with estimated mtDNA coalescence times of 0.99 million years (0.66–1.54 Ma), are located in close proximity (9.6 km) in Lorain County, Ohio, suggesting this is a probable point of secondary contact between divergent groups of populations. In this study, we explored the genetic structure of this putative contact zone using mtDNA and microsatellite loci. Our aim was to quantify the degree of admixture, with possible results ranging from random mating to complete reproductive isolation, and to identify the center and width of the genetic clines. If mtDNA accurately reflects the presence of a secondary contact zone, we hypothesized that microsatellite loci would show similar clinal variation across the sampling transect, though the nuclear loci could vary in their inferred cline widths and centers. Contrary to our hypothesis, we did not

find evidence of a cline in the nuclear data, even though our sampling range was 53 km. We compare our results with other studies of secondary contacts in terrestrial salamanders and discuss the possible explanations for the discordance between mtDNA and the microsatellite loci.

Materials and Methods

Contact Zone Sampling.—We collected tail tips from 316 individuals of *P. cinereus* from 16 sites (mean: 19.8 individuals/site), each visited once, between October 2013 and June 2017 (Table 1; Fig. 1A,B). Tail tips were stored in 95% ethanol, and we released salamanders at the place of capture. Our sampling spans the contact between two clades of *P. cinereus*, which Radomski (2017) referred to as the Ohio (OH) clade (the western portion of our sampling) and the Pennsylvania (PA) clade (the eastern portion of our sampling). Our sample sites 12 and 10, which are 9.6 km apart, represent the OH and PA mtDNA clades, respectively (Radomski, 2017). We sampled an east–west cline because visual examination of clade ranges suggests the PA clade colonized from the east, and the OH clade from the west, and the transect is bounded by Lake Erie to the north. Recent agricultural and suburban development in the area limited dense spatial sampling. A straight-line distance of 53.3 km separates our most widely spaced samples.

Laboratory Procedures.—We extracted DNA from tail tips with the use of Wizard Genomic DNA Purification Kits (Promega, Inc., Madison, Wisconsin, USA). To assign individuals to PA or OH mtDNA clades, we amplified an 845 base-pair region of cytochrome *b* with polymerase chain reaction (PCR; Appendix 1 and 2) and then subjected sequences to restriction fragment length polymorphism (RFLP) analysis (Kuchta, 2007). mtDNA sequence data from localities within and outside of the transect are consistent with eastward expansion of the OH clade, although PA-clade localities show no variation (Radomski, 2017; Supplementary Fig. S1 created in TCS v.1.21; Clement et al., 2000). Therefore, a binary clade assignment was sufficiently informative for mtDNA haplotypes at this scale. We performed the RFLP procedure twice for each individual: the first run used the restriction enzyme AluI, which cut the amplified sequence once for the PA clade and twice for the OH clade; the second run used the restriction enzyme RsaI, which cut the PA sequence twice and the OH sequence once. Procedures for both restriction enzymes were 4 μL dH_2O, 1 μL 1X buffer, 1 μL restriction enzyme, and 4 μL PCR product. We incubated reactions at 37°C for 16 h followed by a 20-min incubation at 65°C, and visualized fragments on 3% agarose gels.

We also amplified 10 microsatellite loci (Cameron et al., 2017). The names of loci and PCR procedures are detailed in Appendixes 3 and 4. We confirmed successful reactions using gel electrophoresis with 3% agarose gels before fragment analysis on an Applied Biosystems 3730 at Arizona State University (Life Technologies, Inc., Waltham, Massachusetts, USA). We conducted our PCR procedures only once upon obtaining successful reactions. To obtain genotypes, BPW and MMH manually assigned peaks and bins using Geneious v.9.1.5 (Kearse et al., 2012). We carefully compared the calls of both researchers to verify consistency.

Microsatellite Quality Control and Summary Statistics.—We assessed microsatellite loci for scoring errors, homozygote excess, and the presence of null alleles using Micro-Checker v.2.2.3 (Van Oosterhout et al., 2004). We calculated the number of alleles, effective number of alleles, number of private alleles, and the observed and expected heterozygosity in GenAlEx v.6.5 (Peakall and Smouse, 2012). We used Genepop v.4.3 (Rousset, 2008) to calculate the Weir and Cockerham (1984) estimates of F_{IS} and to conduct exact tests for departures from Hardy-Weinberg equilibrium (HWE) and genotypic equilibrium, following sequential Bonferroni correction (Holm, 1979). Finally, we used the 'PopGenKit' package (Paquette, 2012) in R v.3.3.3 (R Core Team, 2014) to calculate allelic richness (A_r; number of replicates = 1,000) standardized to the sample size of the smallest sample (site 14; $n = 10$).

Table 1. List of sampling localities with site numbers, names, coordinates, and sample sizes. χ represents the single-coordinate distance of each site along the transect used for the cline analysis (see Appendix 6).

Site	Locality name	Latitude	Longitude	χ (km)	*n*
1	Edison Woods	41.341	−82.489	0	16
2	Schoepfle Garden	41.331	−82.350	11.1	17
3	Mill Hollow Bacon Woods	41.381	−82.321	14.7	20
4	Baumhart Road	41.415	−82.283	18.7	24
5	Crownhill Cemetery	41.395	−82.231	22.4	28
6	Amherst Beaver Creek	41.406	−82.233	22.5	28
7	Kennedy Park	41.426	−82.230	23.2	18
8	Elmwood Park	41.434	−82.173	28.1	20
9	Cromwell Park	41.456	−82.152	30.3	26
10	Cascade Park	41.374	−82.109	31.9	14
11	Black River Reservation	41.416	−82.102	33.5	26
12	James Day Park	41.461	−82.104	34.4	29
13	French Creek	41.460	−82.096	35.0	13
14	Bradley Woods Reservation	41.420	−81.952	45.8	10
15	Huntington Reservation	41.486	−81.934	48.8	13
16	Rocky River Reservation	41.421	−81.859	53.4	14

Microsatellite Genetic Differentiation and Isolation-by-Distance.—We calculated genetic differentiation with locus-specific and pairwise G''_{ST} in GenAlEx v.6.5 with *P*-values estimated from 9,999 permutations. G''_{ST} is a G-statistic that scales G_{ST} from 0.0 to 1.0 and corrects for bias in pairwise comparisons (Meirmans and Hedrick, 2011). Additionally, we calculated G''_{ST} among individuals pooled by mtDNA clade (OH vs. PA).

To test for isolation-by-distance, we conducted a distance-based redundancy analysis (db-RDA; Legendre and Fortin, 2010) in the R package 'vegan' (Oksanen et al., 2017). We used this test to quantify the proportion of variation in a matrix of genetic distances that was explained by geographic coordinates. We calculated genetic distances as pairwise F_{ST} (Weir and Cockerham, 1984) in Genepop (Rousset, 2008). We report adjusted R^2 values to correct for inflation of R^2 in the db-RDA (Bocard et al., 2011).

Microsatellite Population Structure and Hybrid Identification.—We analyzed population structure with the use of three approaches. First, we conducted a discriminant analysis of principle components (DAPC) in the R package 'adegenet' 1.4-2 (Jombart, 2008). DAPC uses *k*-means clustering that maximizes variation between groups after transforming the data with principle components analysis (PCA). We used Bayesian information criteria (BIC) to compare values of *k*. We used cross-validation with 30 replicates, and *a* scores with 10 replicates for each number of retained principle components (PCs), to determine the number of PCs to retain in the analysis, favoring cross validation if discordant (Jombart and Collins, 2015). We also performed DAPC with prior clusters corresponding to sampling localities.

Secondly, we evaluated population structure with STRUCTURE 2.3 (Pritchard et al., 2000), which uses a Bayesian framework to assign individuals to a user-defined number of genetic clusters (*K*) by maximizing conformity to Hardy-Weinberg equilibrium and minimizing linkage disequilibrium.

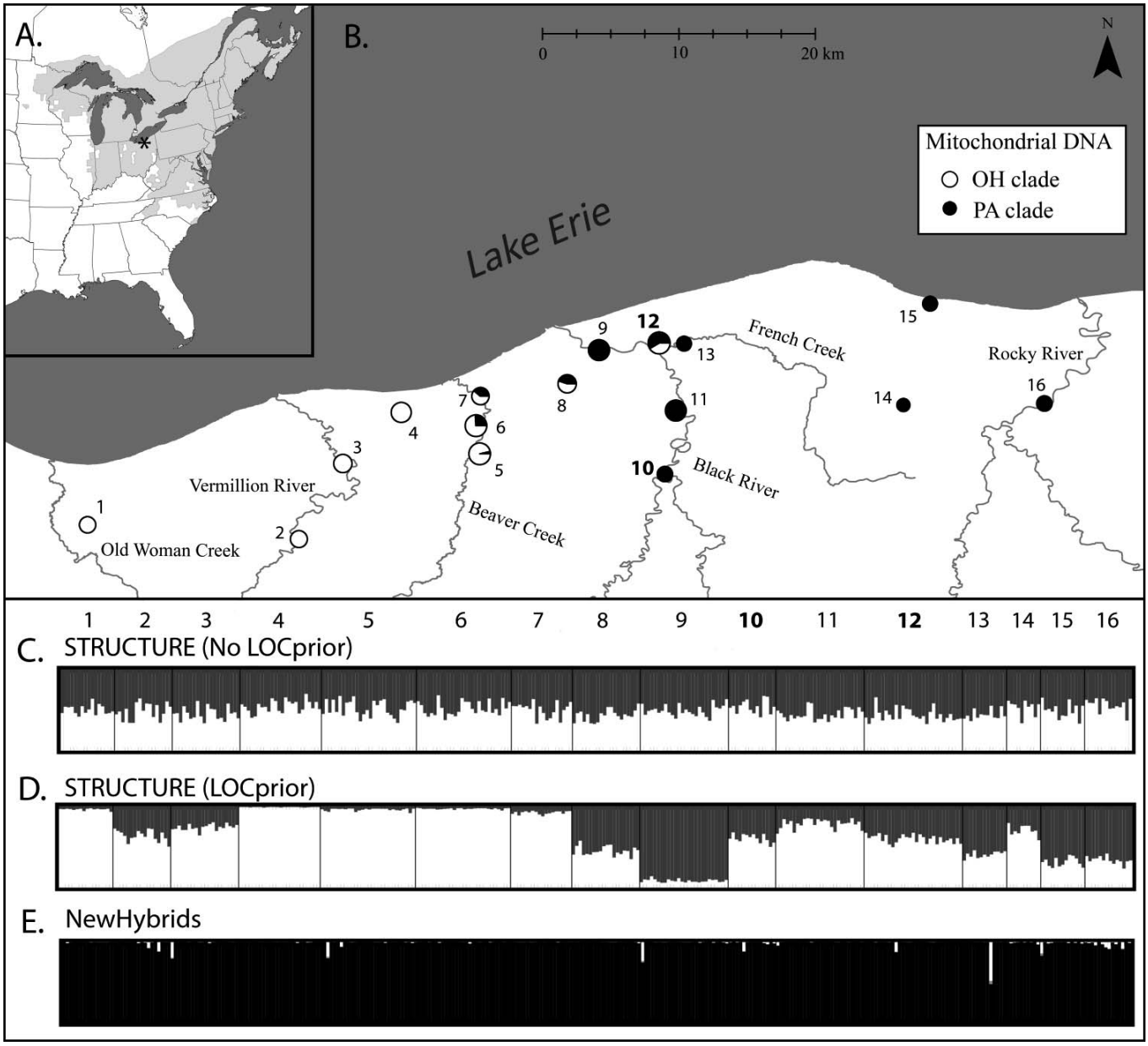

FIG. 1. (A) Map of the eastern United States and Canada with geographic range of *Plethodon cinereus* shaded in light gray (IUCN et al., 2015). The asterisk denotes the sampling region of the contact zone in northern Ohio. (B) Sampling region including 16 localities. Pies represent the proportion of individuals of the OH (white) and PA (black) mtDNA clades discovered at each site, and pie size corresponds to sample size. Notable riverine barriers are labeled; locality numbers are positioned to indicate the side of rivers that sites are located. Sites 10 and 12 in bold were sampled for mtDNA by Radomski (2017), and were designated as PA and OH populations, respectively. (C) STRUCTURE results ($K = 2$) for microsatellite DNA using the admixture model, without incorporating the LOCprior. (D) STRUCTURE results ($K = 2$) using the admixture model and the LOCprior (LOCISPOP). (E) NewHybrids results using uniform priors. Each individual is a vertical bar, and the y-axis indicates an individual's posterior probability of assignment to each genotype class (summing to 1). Black portions of the bar represent the assignment probability to one of two parent populations. White portions represent backcrosses to this first parent population. Probabilities of assignment to all other genotype classes (parent population 2, F1, F2, backcross to parent population 2) are combined and represented by gray, although these combined posterior probabilities are low (<0.04) and generally not visible.

We implemented the admixture model with correlated allele frequencies, and ran the analysis with and without locality data using the LOCprior (LOCISPOP). We conducted 10 independent runs for $K = 1$ to $K = 16$, each with randomly generated seeds, and assessed convergence by comparing results across runs. We ran 700,000 iterations for each Markov chain Monte Carlo (MCMC) and discarded the first 350,000 iterations as burn-in (Converse et al., 2017). We used Structure Harvester web v.0.6.94 (Earl and von Holdt, 2012) to calculate ΔK using the Evanno method (Evanno et al., 2005); then we visualized results with the use of CLUMPP v.1.1.2 (Jakobsson and Rosenberg, 2007) and Distruct v.1.1 (Rosenberg, 2004). Because ΔK detects the basal level of structure (Evanno et al., 2005), we ran STRUCTURE hierarchically to test for substructure within clusters (Converse et al., 2017; Janes et al., 2017). Finally, we used a spatially explicit Bayesian model in TESS v.2.3.1 (Durand et al., 2009) to estimate the number of clusters and admixture proportions. Results from TESS did not reveal further genetic structure compared to DAPC or STRUCTURE, so we present the methods and results for TESS in Figure S2.

TABLE 2. Summary statistics (±SE) across 10 microsatellite loci at each of 16 sites. Number of alleles, effective number of alleles (N_e), and private alleles are summed across all 10 loci. Observed and expected heterozygosity (H_O and H_E), the Weir and Cockerham (1984) inbreeding coefficient (F_{IS}), and allelic richness (A_r) represent averages at each site.

Site	No. of alleles	N_e	Private alleles	H_O	H_E	F_{IS}	A_r
1	32	21.6	1	0.28 ± 0.1	0.30 ± 0.1	0.1 ± 0.07	2.9 ± 0.8
2	37	19.3	3	0.35 ± 0.1	0.34 ± 0.08	0.01 ± 0.1	3.1 ± 0.5
3	29	17.8	2	0.25 ± 0.09	0.26 ± 0.08	0.18 ± 0.13	2.5 ± 0.6
4	34	22.4	0	0.32 ± 0.1	0.32 ± 0.1	−0.01 ± 0.06	2.9 ± 0.8
5	44	24.1	1	0.33 ± 0.1	0.34 ± 0.1	0.04 ± 0.03	3.3 ± 0.9
6	41	22.7	1	0.29 ± 0.09	0.30 ± 0.1	0.06 ± 0.07	3.0 ± 0.8
7	29	19.6	0	0.31 ± 0.08	0.32 ± 0.09	0.05 ± 0.06	2.6 ± 0.7
8	35	19.6	1	0.31 ± 0.11	0.27 ± 0.1	−0.1 ± 0.04	2.8 ± 0.7
9	33	20.5	1	0.37 ± 0.1	0.35 ± 0.09	−0.06 ± 0.07	2.7 ± 0.6
10	39	21.8	2	0.34 ± 0.07	0.38 ± 0.09	0.08 ± 0.1	3.5 ± 0.7
11	37	18.6	2	0.23 ± 0.09	0.26 ± 0.1	0.13 ± 0.08	2.8 ± 0.6
12	33	17.8	1	0.29 ± 0.1	0.30 ± 0.09	0.08 ± 0.08	2.7 ± 0.5
13	31	18.9	1	0.30 ± 0.09	0.30 ± 0.09	0.02 ± 0.09	2.9 ± 0.6
14	36	21.9	1	0.36 ± 0.09	0.35 ± 0.09	0.00 ± 0.05	N/A
15	35	21.0	0	0.41 ± 0.09	0.38 ± 0.08	−0.06 ± 0.05	3.3 ± 0.7
16	43	24.6	3	0.44 ± 0.1	0.4 ± 0.09	−0.07 ± 0.06	3.8 ± 0.9

To identify hybrid individuals, we used NewHybrids v.1.1, which estimates the posterior probability of each individual belonging to distinct genotype frequency classes (Anderson and Thompson, 2002). We used the default classes of pure parentals, F1, F2, and backcrosses. We tested both Jeffrey's and uniform priors for mixing parameters and allele frequencies. For both priors, we performed five independent runs, each with 200,000 iterations discarded as burn-in followed by 1,000,000 iterations for analysis, and compared runs for convergence.

MtDNA Cline Analyses.—Because microsatellite loci did not exhibit fixed differences between clades, we used the R package 'INTROGRESS' (Gompert and Buerkle, 2010) to assign alleles to either clade, using sites 1 and 16 as reference populations for the OH and PA clades, respectively. Results from INTROGRESS (Appendix 5), STRUCTURE, DAPC, TESS, and NewHybrids, however, indicate that microsatellite variation does not support the presence of two clades (see results), and we were unable to determine which clade (OH or PA) the microsatellite DNA represented. In addition, when we divided individuals into groups based on mtDNA clade, the most common microsatellite alleles were the same for 9/10 loci. Therefore, we performed a cline analysis using only mtDNA haplotypes with the R-package 'HZAR' v.0.2-5 (Derryberry et al., 2014), that fits data to cline models with a Metropolis-Hastings algorithm. We detail cline-fitting methods in Appendix 6.

Finally, we quantified the strength of selection on mtDNA under a tension zone model, assuming that the width of the mtDNA cline reflects a balance between gene flow into the hybrid zone and selection against hybrids (a tension zone). The strength of selection, s, is proportional to cline width, w, and dispersal, σ (standard deviation of parent-offspring distance), where $s = 8\sigma^2/w^2$ (Bazykin, 1969; Alexandrino et al., 2005). We tested our best-fit cline width values along with dispersal values of both $\sigma = 20$ m, as studies have estimated dispersal distances <20 m (Cabe et al., 2007; Grant and Liebgold, 2017), and $\sigma = 80$ m, the latter proposed as the yearly rate of expansion during post-Pleistocene expansion (Cabe et al., 2007).

RESULTS

MtDNA Genotyping, Microsatellite Quality Control, and Summary Statistics.—Of the 316 cytochrome *b* haplotypes, 159 were OH clade and 157 were PA clade (Fig. 1B). Most populations were fixed for one haplotype, but five sites (5, 6, 7, 8, 12) contained both OH and PA haplotypes. Site 9 contained only PA-clade haplotypes despite being geographically intermediate to sites 8 and 12, both of which contained both haplotypes.

For microsatellites, there was no evidence for deviations from HWE or for genotypic linkage disequilibrium after sequential Bonferroni correction. Micro-Checker detected evidence for homozygote excess and null alleles in PC7 (site 11), PC25 (6, 10, 13), and PC37 (3). We retained these loci, but their exclusion did not affect our analyses (results not shown). Across all loci and sites, we recovered 85 alleles, ranging from 3 (PC30 and PC37) to 21 (PC25) alleles per locus (Table 2; summary statistics for each locus based on mtDNA clade membership and sampling locality in Appendix 7 and Supplementary Table S1, respectively). Although some loci had low allelic diversity or were fixed for a single allele at most sites (e.g., PC30), tests for genetic differentiation and structure yielded qualitatively identical results when the four most allele-poor loci were dropped from analyses (results not shown). Therefore, we retained all loci in subsequent analyses.

Microsatellite Genetic Differentiation and Isolation-by-Distance.—Locus-specific estimates of G''_{ST} ranged from −0.003 to 0.201. All loci except PC37 exhibited significant differentiation after Bonferroni correction. Pairwise estimates of G''_{ST} ranged from −0.008 (sites 2 and 14) to 0.239 (3 and 9), and 64 of the 120 comparisons were significant after Bonferroni correction (Table 3). When we grouped individuals based on their mtDNA clade, microsatellite differentiation was low, but significant ($G''_{ST} = 0.03$; $P < 0.001$). The db-RDA did not support the hypothesis of isolation-by-distance: adjusted R^2 indicated geographic distance accounted for 15.8% of the variation in F_{ST}, but this relationship was not significant ($P = 0.08$; see Fig. S3 for a scatterplot of pairwise F_{ST} and geographic distance).

Microsatellite Population Structure and Hybrid Identification.—With our microsatellite data, DAPC did not reveal genetic clusters that correspond to clade membership or geographic proximity. BIC scores did not suggest a clear number of clusters in the data (Fig. S4), and across *K*-values clusters overlapped considerably (we show $K = 6$ in Fig. 2A). Individuals of either mtDNA clade appeared evenly distributed among these clusters

TABLE 3. Pairwise comparisons of sampling localities for the Meirmans and Hedrick (2011) G''_{ST}. Values in bold are significant at $P < 0.05$ after sequential Bonferroni correction.

	1	2	3	4	5	6	7	8	9	10	11	12	13	14	15	16
1	–	**0.078**	**0.074**	0.029	0.012	0.022	0.018	**0.112**	**0.205**	0.052	0.067	0.049	**0.113**	0.095	0.065	**0.118**
2		–	0.049	**0.073**	0.048	**0.090**	0.059	0.035	**0.139**	0.014	0.030	**0.057**	**0.093**	–0.008	0.022	0.039
3			–	**0.096**	**0.090**	**0.135**	**0.085**	**0.075**	**0.239**	0.036	0.046	**0.072**	**0.137**	0.047	**0.089**	**0.080**
4				–	0.019	0.027	**0.061**	**0.108**	**0.203**	0.054	**0.062**	**0.063**	**0.096**	0.061	**0.094**	**0.100**
5					–	0.027	0.019	**0.087**	**0.160**	0.047	**0.053**	**0.062**	0.065	0.066	0.061	**0.099**
6						–	0.047	**0.153**	**0.174**	0.065	**0.115**	**0.091**	**0.125**	**0.113**	**0.095**	**0.141**
7							–	**0.125**	**0.168**	0.015	**0.082**	**0.074**	**0.124**	0.060	0.051	**0.096**
8								–	**0.166**	**0.089**	0.029	0.047	0.024	0.052	0.050	**0.093**
9									–	**0.136**	**0.186**	**0.163**	**0.116**	**0.176**	**0.090**	**0.159**
10										–	0.061	0.055	**0.121**	0.003	0.017	0.005
11											–	**0.051**	**0.075**	0.053	0.070	**0.077**
12												–	0.042	0.069	0.031	**0.090**
13													–	0.106	0.060	**0.127**
14														–	0.041	0.007
15															–	0.026
16																–

(Fig. 2B). When clustering by sampling locality, clusters largely overlapped, with the possible exception of sites 9 and 16 (Fig. S5).

Without the LOCprior, STRUCTURE did not detect any population structure (Fig. 1C), a result corroborated by TESS across several models and *K*-values (Fig. S2). When using the LOCprior, STRUCTURE found an optimal solution at $\Delta K = 2$ using the Evanno method. These two groups form weakly differentiated eastern and western clusters (Fig. 1D). The western group included five sample sites with low levels of admixture (average ancestry coefficient (q) $\geq$ 0.919; sites 1, 4, 5, 6, 7), whereas site 9 accounted for the only eastern group locality with limited admixture (q = 0.915). The remaining 10 populations were either highly admixed, or STRUCTURE was unable to assign individuals to either group with confidence. When we repeated STRUCTURE within the western group, we did not detect substructure. We did not analyze the eastern group, because all sites except site 9 were highly admixed; however, we also analyzed the results of $K = 3$ with all 16 sites and observed similar structure as $K = 2$, except the eastern group was divided into two clusters (Fig. S2). The LOCprior model hints at the possibility of two or three genetic groups within our range of sampling, but this is not corroborated by other analyses, and no analysis indicates a cline, as expected from a hybrid zone.

Using NewHybrids with Jeffrey's priors, we failed to obtain consistent results when the starting seeds were altered among successive runs, suggesting the prior was not appropriate. With uniform priors, 308 individuals had a posterior probability >0.9 of belonging to a single pure parental population, whereas the remaining 8 individuals had some posterior probability of being backcrosses to this parental population, although probabilities of backcrossing were all <0.5 (0.11–0.47), suggesting evidence of backcrossing is not well supported. We did not find putative backcrosses at a single locality or geographic region (Fig. 1E), but were distributed among populations. Therefore, NewHybrids did not provide compelling evidence of a hybrid zone within our sampling range.

MtDNA Cline Analyses.—In contrast with the microsatellite data, mtDNA showed good evidence of a cline: all five cline models outperformed the null model of no cline (all ΔAICc > 241.3; Table 4). The model with the lowest AICc value (AICc = 62.6) was the right-tailed model, with c = 23.5 km, and w = 2.1 km, although estimates for the parameters relating to the introgression tail (δ_R and τ_R) were variable (Table 4). The two log-likelihood support limits for both c (23.0–27.4 km) and w (0.9–10.9 km) overlapped support limits of the no-tail model (ΔAICc = 6.0; c = 27.3 km; w = 11.6 km; Table 4; Fig. 3). These estimates indicate that the cline center is situated between sites 6 and 8; however, sites 8–13 fall outside of the 95% credible region (Fig. 3), suggesting that the model may not accurately reflect the cline center, perhaps because calculations were based on a one-dimensional cline model. Our estimates for selection strength indicated little to no selection: assuming σ = 20 m, s = 0.07% (0.00–0.40%, based on the two log-likelihood width estimates); assuming σ = 80 m, the selection strength increases modestly to 1.16% (0.04–6.32%).

DISCUSSION

In this study, we sought to characterize a hybrid zone identified with the use of mtDNA by using nuclear markers. Northern Ohio possesses a postglacial landscape, so the hybrid zone must have formed relatively recently (Radomski, 2017). Our sampling transect captured the mtDNA cline, with five localities containing both mtDNA clades. We found a best-fit mtDNA cline width of 2.1 km (0.9–10.9 km), which is comparable to the width of another *P. cinereus* contact zone on

TABLE 4. Cline fitting summary and parameter estimates. Two log-likelihood support units are listed in parentheses below each parameter estimate. δ and τ represent the shape parameters for left and right tails.

Model	AICc	ΔAICc	LL	Center (km)	Width (km)	δ_L	τ_L	δ_R	τ_R
Null model	314.1	251.5	−156.1	–	–	–	–	–	–
No tails	68.7	6.0	−32.3	27.3 (26.2–28.4)	11.6 (9.4–14.6)	–	–	–	–
Right tail	62.6	–	−27.3	23.5 (23.0–27.4)	2.1 (0.9–10.9)	–	–	0.0 (0.0–5.3)	0.1 (0.0–0.6)
Left tail	72.8	10.2	−32.3	27.3 (26.2–28.4)	11.6 (9.4–14.6)	51.2 (1.5–53.2)	0.2 (0.0–1.0)	–	–
Mirrored tails	69.0	6.4	−30.4	28.1 (26.0–28.7)	5.1 (0.9–12.2)	1.9 (0.0–53.2)	0.2 (0.0–1.0)	1.9 (0.0–53.2)	0.2 (0.0–1.0)
Two tails	66.8	4.2	−27.3	23.5 (22.9–27.8)	1.9 (0.9–10.9)	0.7 (0.0–53.2)	0.7 (0.0–1.0)	0.0 (0.0–5.3)	0.1 (0.0–0.6)

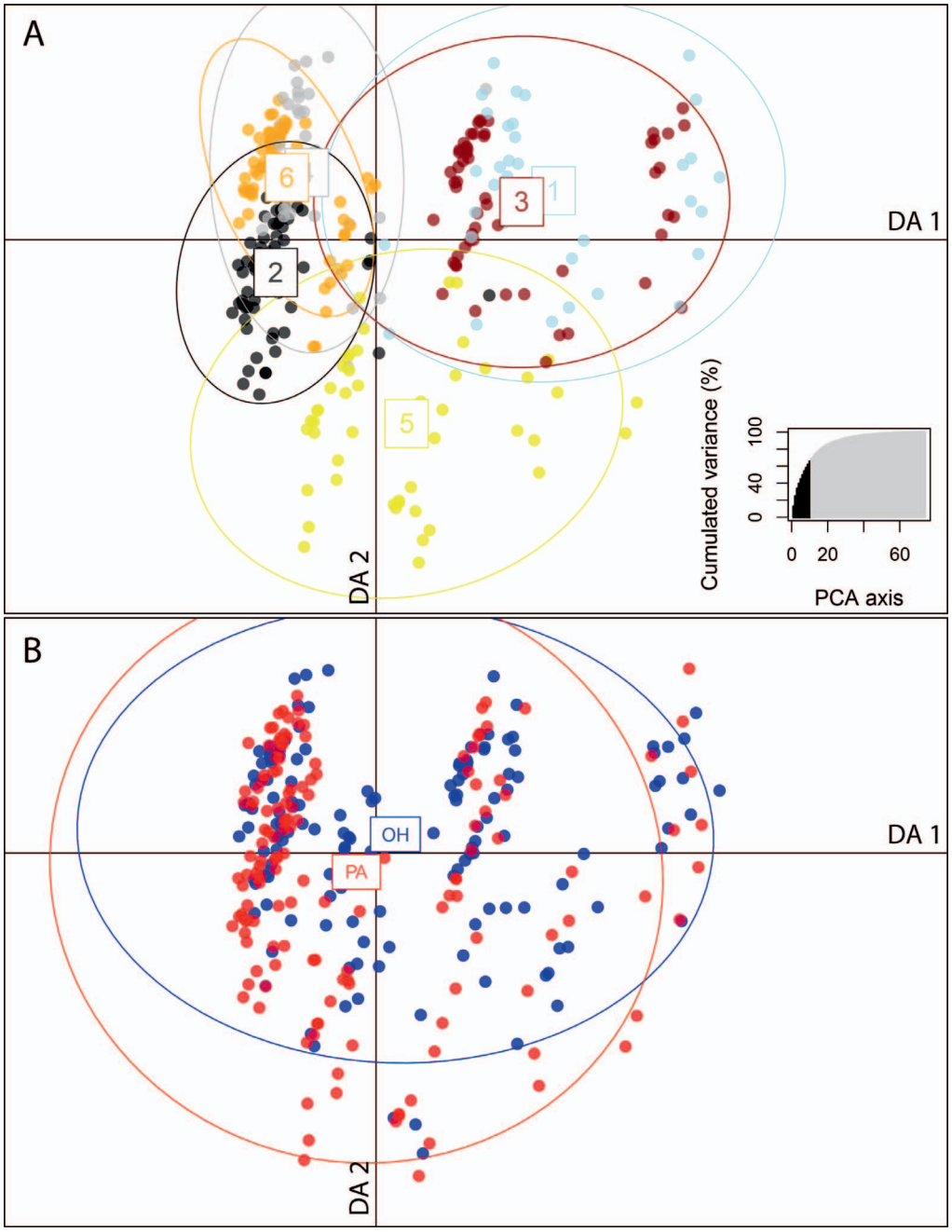

FIG. 2. (A) Discriminant analysis of principle components (DAPC) of microsatellite data when assuming six clusters and retaining 10 PCs and five discriminant functions. BIC values did not demonstrate a clear number of clusters (Supplemental Fig. S4), but other values from $K = 3$–10 did not provide more (or less) useful summaries of the data. The x- and y-axes represent the first and second discriminant axes (DA), respectively. Ellipses are set to approximate a 95% confidence interval (ellipse = 2.5). Inset displays cumulated variance (%) explained against the number of retained PCs. (B) Scatterplot of the same data as (A), but individuals are labeled as OH (blue) and PA (red) mtDNA clade. Note that mtDNA clade membership was not used in clustering analysis; these results simply display mtDNA clade onto the DAPC of $K = 6$.

the Delmarva Peninsula. There, allozymes showed free gene flow between groups that likely colonized from the north and south (Wynn, 1986). Because cline widths are a function of dispersal rates and selection against hybrids or, in the case of neutral clines, time since secondary contact (Barton and Hewitt, 1985), this suggests weak selection, or a similar time since secondary contact. Assuming a tension zone model, we estimated selection strengths from 0.00 to 6.32%. These simple calculations, though they include considerable uncertainty, differ greatly from other estimates, such as the hybrid zone between *Ensatina eschscholtzii xanthoptica* and *Ensatina eschscholtzii platensis* (s = 46–75% with cline widths 730–2000 m; Alexandrino et al., 2005), or that of the yellow-rumped warbler (*Dendroica coronata*; s = 18%; Brelsford and Irwin, 2009). In addition to relatively weak selection in our hybrid zone, there may be no assortative mating: a recent study found no difference in male preference for female sex pheromones of the OH or PA clade, nor did their pheromone profiles differ significantly (Baggett, 2016).

Although mtDNA would suggest a neutral cline, our microsatellite results do not diagnose a cline or a hybrid zone. A diversity of analyses suggests that all or most individuals from

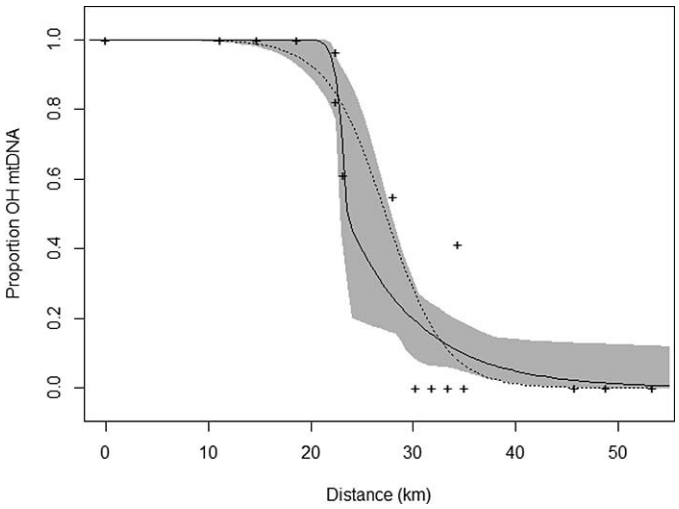

FIG. 3. Geographic cline for mtDNA haplotype frequencies. The x-axis represents distance, χ (km), from our westernmost site along the single-coordinate cline axis; the y-axis represents the proportion of individuals at each site assigned to the OH clade. The solid line is the best-fit, right-tailed model, and the surrounding grey region represents the 95% credible cline region. The dashed line represents the simple, no-tailed model. Although the right-tailed model had the lowest AICc score, the 95% credible region overlapped with the simple cline model, and two log-likelihood estimates showed wide variation in parameter estimates for the right-tailed model.

across the range of our sampling represented a single parental type. Similarly, most analyses suggested no population structure in the transect. The exception is that two or three weakly divergent groups were present when a location prior was used in STRUCTURE; however, these groups do not present a clear cline, as expected in the middle of a hybrid zone, and seem to be the result of subtle population structure rather than secondary contact. Our patterns of nuclear variation resemble other northern populations of *P. cinereus*, which possess weak population structure and a lack of isolation-by-distance as a consequence of post-Pleistocene population expansion (Highton and Webster, 1976; Jordan et al., 2009; Radomski, 2017).

Though we detected little microsatellite genetic structure, patterns of genetic differentiation suggest that PA-clade populations that dispersed into Ohio along Lake Erie may have founded some of the coastal populations. Site 9, which is in the middle of the transect but near the coast of Lake Erie, possessed relatively high genetic differentiation in pairwise comparisons, and also included mtDNA haplotypes ($n = 26$) from only the PA clade despite localities containing both haplotypes to the east and west (as close as 4 km away). Site 9 clusters most closely with, and is the least genetically differentiated from, 15, which is also located along the coast of Lake Erie. Wider sampling and population-genetic analyses with more loci are necessary to infer colonization routes.

We observed a cline consistent with a hybrid zone with mtDNA; however, microsatellite variation supports the presence of only a single genetic population throughout our transect. The conflicting patterns of mtDNA and microsatellites suggest that we have uncovered an example of mitonuclear discordance, in which cline centers or widths differ between the two types of markers (Toews and Brelsford, 2012). Studies of hybrid zones in other terrestrial salamanders provide examples of both concordant and discordant clines. For instance, in the ring species *Ensatina eschscholtzii*, studies of the hybrid zone between *E. e. xanthoptica* and *E. e. platensis* show coincident clines, and between *Ensatina eschscholtzii eschscholtzii* and *Ensatina eschscholtzii klauberi* there is a relatively small discordance of ~100 m (Alexandrino et al., 2005; Devitt et al., 2011). Similarly, Kuchta (2007) found coincident cline centers between mtDNA and allozyme markers in a hybrid zone between the Pacific Newts *Taricha torosa* and *Taricha sierrae*. Concordance or minor discordance is common, but some studies have documented more exaggerated discordance. For instance, between distantly related clades of *E. e. platensis* there is a discordance of ~50–75 km between nuclear and mtDNA cline centers (Kuchta et al., 2009).

The unique properties of mtDNA (e.g., haploid, maternally inherited, lack of recombination, independence from nuclear genome) can affect its patterns in phylogeography and hybrid zone analysis, and the mitonuclear discordance in our transect suggests two possible scenarios. First, the cline in mtDNA may not be the result of secondary contact, or a recent lineage merger has obscured the signal of secondary contact for nuclear DNA. Second, there may be a nuclear cline, but it lies outside of our sampling transect. In the first scenario, the OH and PA mtDNA phylogeographic break may have formed as an artifact of genetic drift rather than secondary contact. Phylogeographic breaks for other taxa are not known in this area, and simulations show that with large effective population sizes and low dispersal, arbitrary phylogeographic breaks in mtDNA can form without historical allopatry (Irwin, 2002), although a dearth of clear examples suggests it is rare. Alternatively, the phylogeographic break may reflect ancient allopatry succeeded by secondary contact and lineage merger, in which the microsatellite cline is far wider than our sampling and so not detectable. Some studies have posited that mtDNA can reflect historical processes, such as divergence in multiple refugia or past introgression, whereas nuclear markers more closely track the current demographic dynamics (Jockusch and Wake, 2002; Weisrock et al., 2005; Edgington et al., 2016). Further, by not selecting loci a priori with known clade-specific alleles (e.g., Alexandrino et al., 2005; Kuchta, 2007), we may not have been able to recover a subtle nuclear cline within our transect, although INTROGRESS suggests that none of our 10 loci are consistent with a cline or secondary contact.

The second scenario, in which a nuclear cline lies outside of our transect, would be a drastic example of noncoincident nuclear and mtDNA cline centers. Historical processes can lead to this pattern as well, if mtDNA reflects the point of ancient secondary contact followed by hybrid zone movement (Jockusch and Wake, 2002). Alternatively, adaptive introgression of mtDNA from one clade to the second could lead to noncoincident cline centers, as mtDNA may be under selection independently from the nuclear genome (Ballard and Whitlock, 2004). Although a number of other possible causes of noncoincident cline centers remain (Toews and Brelsford, 2012), wider sampling with nuclear markers would allow us to determine first if mtDNA represents a true secondary contact zone.

The discordance among loci that we recorded in this study highlights the value of examining multiple data sets. Mitonuclear discordance may evolve through several mechanisms, and a nuclear cline could lie outside of our sampling range. Alternatively, we may have identified yet another example of secondary contact in a postglacial landscape followed by lineage merger, which may be ongoing (Jokusch and Wake, 2002; Richmond and Jockusch, 2007). More work involving wider sampling and genomic resources is needed to evaluate competing hypotheses and develop a clearer understanding of the evolutionary dynamics operating in this possible secondary contact in *P. cinereus*.

Acknowledgments.—We thank our hard-working field assistants: C. Baggett, A. Cameron, M. Ganzfried, J. Laterza-Barbosa, and D. Thiry. Funding was supported by a Grant-in-Aid of Research from Sigma Xi, a Gaige Award from the American Society of Ichthyologists and Herpetologists, and John Carroll University. We obtained permits from the Ohio Department of Natural Resources (Permit 19-012) and Lorain County Metroparks (Black River Reservation Park Use Permit). We thank P. E. Bartelt, R. G. Reynolds, and two anonymous reviewers for helpful comments on an earlier version of this manuscript.

Literature Cited

Alexandrino, J., S. J. Baird, L. Lawson, J. R. Macey, C. Moritz, and D. B. Wake. 2005. Strong selection against hybrids at a hybrid zone in the *Ensatina* ring species complex and its evolutionary implications. Evolution 59:1334–1347.

Anderson, E. C., and E. A. Thompson. 2002. A model-based method for identifying species hybrids using multilocus data. Genetics 160: 1217–1229.

Baggett, C. L. 2016. Population-Level Variation in a Pheromone Complex across Species' Geographic Range. Unpublished M.S. thesis, John Carroll University, University Heights, Ohio, USA.

Ballard, J. W. O., and M. C. Whitlock. 2004. The incomplete natural history of mitochondria. Molecular Ecology 13:729–744.

Barton, N. H., and G. M. Hewitt. 1985. Analysis of hybrid zones. Annual Review of Ecology and Systematics 16:113–148.

Barton, N. H., and G. M. Hewitt. 1989. Adaptation, speciation and hybrid zones. Nature 341:497–305.

Bazykin, A. D. 1969. Hypothetical mechanism of speciation. Evolution 23:685–687.

Bocard, D., F. Gillet, and P. Legendre. 2011. Numerical Ecology with R. Springer, USA.

Brelsford, A., and D. E. Irwin. 2009. Incipient speciation despite little assortative mating: the yellow-rumped warbler hybrid zone. Evolution 63:3050–3060.

Burton, T. M., and G. E. Likens. 1975. Salamander populations and biomass in the Hubbard Brook experimental forest, New Hampshire. Copeia 1975:541–546.

Cabe, P. R., R. B. Page, T. J. Hanlon, M. E. Aldrich, L. Connors, and D. M. Marsh. 2007. Fine-scale population differentiation and gene flow in a terrestrial salamander (*Plethodon cinereus*) living in continuous habitat. Heredity 98:53–60.

Cameron, A. C., J. J. Anderson, and R. B. Page. 2017. Assessment of intra and interregional genetic variation in the eastern red-backed salamander, *Plethodon cinereus*, via analysis of novel microsatellite markers. PloS One 12:e0186866.

Clement, M., D. Posada, and K. Crandall. 2000. TCS: a computer program to estimate gene genealogies. Molecular Ecology 9:657–1660.

Converse, P. E., S. R. Kuchta., J. S. Hauswaldt, and W. M. Roosenburg. 2017. Turtle soup, Prohibition, and the population genetic structure of diamondback terrapins (*Malaclemys terrapin*). PloS One 12:e0181898.

Derryberry, E. P., G. E. Derryberry, J. M. Maley, and R. T. Brumfield. 2014. Hzar: hybrid zone analysis using an R software package. Molecular Ecology Resources 14:652–663.

Devitt, T. J., S. J. Baird, and C. Moritz. 2011. Asymmetric reproductive isolation between terminal forms of the salamander ring species *Ensatina eschscholtzii* revealed by fine-scale genetic analysis of a hybrid zone. BMC Evolutionary Biology 11:245.

Durand, E., F. Jay, O. E. Gaggiotti, and O. François. 2009. Spatial inference of admixture proportions and secondary contact zones. Molecular Biology and Evolution 26:1963–1973.

Dyke, A. S. 2004. An outline of North American deglaciation with emphasis on central and northern Canada. Developments in Quaternary Sciences 2:373–424.

Earl, D. A., and B. M. von Holdt. 2012. STRUCTURE HARVESTER: a website and program for visualizing STRUCTURE output and implementing the Evanno method. Conservation Genetics Resources 4:359–361.

Edgington, H. A., C. M. Ingram, and D. R. Taylor. 2016. Cyto-nuclear discordance suggests complex evolutionary history in the cave-dwelling salamander, *Eurycea lucifuga*. Ecology and Evolution 6: 6121–6138.

Edwards, S. V. 2009. Is a new and general theory of molecular systematics emerging? Evolution 63:1–19.

Evanno, G., S. Regnaut, and J. Goudet. 2005. Detecting the number of clusters of individuals using the software STRUCTURE: a simulation study. Molecular Ecology 14:2611–2620.

Gay, L., P. A. Crochet, D. A. Bell, and T. Lenormand. 2008. Comparing clines on molecular and phenotypic traits in hybrid zones: a window on tension zone models. Evolution 62:2789–2806.

Gompert, Z., and C. Alex Buerkle. 2010. INTROGRESS: a software package for mapping components of isolation in hybrids. Molecular Ecology Resources 10:378–384.

Grant, A. H., and E. B. Liebgold. 2017. Color-biased dispersal inferred by fine-scale genetic spatial autocorrelation in a color polymorphic salamander. Journal of Heredity 108:588–593.

Harrison, R. G. (Ed.). 1993. Hybrid Zones and the Evolutionary Process. Oxford University Press, USA.

Hass, C. A. 1985. Geographic Protein Variation in the Red-Backed Salamander (*Plethodon cinereus* [Green]) from the Southern Part of its Range. M.S. thesis. University of Maryland, College Park, Maryland, USA.

Highton, R. 1999. Hybridization in the contact zone between *Plethodon richmondi* and *Plethodon electromorphus* in northern Kentucky. Herpetologica 55:91–105.

Highton, R., and T. P. Webster. 1976. Geographic protein variation and divergence in populations of the salamander *Plethodon cinereus*. Evolution 30:33–45.

Holm, S. 1979. A simple sequentially rejective multiple test procedure. Scandinavian Journal of Statistics 6:65–70.

Irwin, D. E. 2002. Phylogeographic breaks without geographic barriers to gene flow. Evolution 56:2383–2394.

IUCN, Conservation International, and NatureServe. 2015. *Plethodon cinereus* species range. http://maps.iucnredlist.org/map.html?id=59334. Accessed 2 June 2018.

Jakobsson, M., and N. A. Rosenberg. 2007. CLUMPP: a cluster matching and permutation program for dealing with label switching and multimodality in analysis of population structure. Bioinformatics 23: 1801–1806.

Janes, J. K., J. M. Miller, J. R. Dupuis, R. M. Malenfant, J. C. Gorrell, C. I. Cullingham, and R. L. Andrew. 2017. The $K = 2$ conundrum. Molecular Ecology 26:3594–3602.

Jockusch, E. L., and D. B. Wake. 2002. Falling apart and merging: diversification of slender salamanders (Plethodontidae: *Batrachoseps*) in the American West. Biological Journal of the Linnean Society 76: 361–391.

Jombart, T. 2008. Adegenet: a R package for the multivariate analysis of genetic markers. Bioinformatics 24:1403–1405.

Jombart, T., and C. Collins. 2015. A tutorial for discriminant analysis of principal components (DAPC) using adegenet 2.0.0. Available from: http://adegenet.r-forge.r-project.org/files/tutorial-dapc.pdf

Jordan, M. A., D. A. Morris, and S. E. Gibson. 2009. The influence of historical landscape change on genetic variation and population structure of a terrestrial salamander (*Plethodon cinereus*). Conservation Genetics 10:1647–1658.

Kearse, M., R. Moir, A. Wilson, S. Stones-Havas, M. Cheung, S. Sturrock, S. Buxton, A. Cooper, S. Markowitz, C. Duran, T. Thierer, B. Ashton, P. Mentjies, and A. Drummond. 2012. Geneious Basic: an integrated and extendable desktop software platform for the organization and analysis of sequence data. Bioinformatics 28:1647–1649.

Kuchta, S. R. 2007. Contact zones and species limits: hybridization between lineages of the California newt, *Taricha torosa*, in the southern Sierra Nevada. Herpetologica 63:332–350.

Kuchta, S. R., D. S. Parks, R. L. Mueller, and D. B Wake. 2009. Closing the ring: historical biogeography of the salamander ring species *Ensatina eschscholtzii*. Journal of Biogeography 36:982–995.

Lee-Yaw, J. A., J. T. Irwin, and D. M. Green. 2008. Postglacial range expansion from northern refugia by the wood frog, *Rana sylvatica*. Molecular Ecology 17:867–884.

Legendre, P., and M. J. Fortin. 2010. Comparison of the Mantel test and alternative approaches for detecting complex multivariate relationships in the spatial analysis of genetic data. Molecular Ecology Resources 10:831–844.

Martínez-Solano, I., E. L. Jockusch, and D. B. Wake. 2007. Extreme population subdivision throughout a continuous range: phylogeography of *Batrachoseps attenuatus* (Caudata: Plethodontidae) in western North America. Molecular Ecology 16:4335–4355.

Meirmans, P. G., and P. W. Hedrick. 2011. Assessing population structure: F_{ST} and related measures. Molecular Ecology Resources 11:5–18.

NEWMAN, C. E., AND C. C. AUSTIN. 2015. Thriving in the cold: glacial expansion and post-glacial contraction of a temperate terrestrial salamander (*Plethodon serratus*). PloS One 10:e0130131.
OKSANEN, J., R. KINDT, P. LEGENDRE, B. O'HARA, G. L. SIMPSON, P. SOLYMOS, M. H. H. STEVENS, AND H. WAGNER. 2017. The vegan package. Community ecology package. Available at: http://CRAN.R-project.org/package=vegan.
PAQUETTE, S. R. 2012. PopGenKit: Useful functions for (batch) file conversion and data resampling in microsatellite datasets. R package version, 1.
PEAKALL, R., AND P. E. SMOUSE. 2012. GenALEx 6.5: genetic analysis in Excel. Population genetic software for teaching and research—an update. Bioinformatics 28:2537–2539.
PRITCHARD, J. K., M. STEPHENS, AND P. DONNELLY. 2000. Inference of population structure using multilocus genotype data. Genetics 155: 945–959.
R CORE TEAM. 2014. R: A Language and Environment for Statistical Computing. R Foundation for Statistical Computing, Austria.
RADOMSKI, T. P. 2017. Biogeography and Climatic Niche Evolution in the Eastern Red-Backed Salamander. M.S. thesis, Ohio University, Athens, Ohio, USA.
RICHMOND, J. Q., AND E. L. JOCKUSCH. 2007. Body size evolution simultaneously creates and collapses species boundaries in a clade of scincid lizards. Proceedings of Biological Sciences 274:1701–1708.
RIEUX, A., T. LENORMAND, J. CARLIER, L. DE LAPEYRE DE BELLAIRE, AND V. RAVIGNÉ. 2013. Using neutral cline decay to estimate contemporary dispersal: a generic tool and its application to a major crop pathogen. Ecology Letters 16:721–730.
ROSENBERG, N. 2004. DISTRUCT: a program for the graphical display of population structure. Molecular Ecology Notes 4:137–138.
ROUSSET, F. 2008. GENEPOP'007: A complete re-implementation of the GENEPOP software for Windows and Linux. Molecular Ecology Resources 8:103–106.
THESING, B. D., R. D. NOYES, D. E. STARKEY, AND D. B. SHEPARD. 2016. Pleistocene climatic fluctuations explain the disjunct distribution and complex phylogeographic structure of the southern red-backed salamander, *Plethodon serratus*. Evolutionary Ecology 30:89–104.
TOEWS, D. P. L., AND A. BRELSFORD. 2012. The biogeography of mitochondrial and nuclear discordance in animals. Molecular Ecology 21:3907–3930.
VAN OOSTERHOUT, C., W. F. HUTCHINSON, D. P. WILLS, AND P. SHIPLEY. 2004. MICRO-CHECKER: software for identifying and correcting genotyping errors in microsatellite data. Molecular Ecology Notes 4:535–538.
WEIR, B. S., AND C. C. COCKERHAM. 1984. Estimating F-statistics for the analysis of population structure. Evolution 38:1358–1370.
WEISROCK, D. W., K. H. KOZAK, AND A. LARSON. 2005. Phylogeographic analysis of mitochondrial gene flow and introgression in the salamander, *Plethodon shermani*. Molecular Ecology, 14:1457–1472.
WYNN, A. H. 1986. Linkage disequilibrium and a contact zone in *Plethodon cinereus* on the Del-Mar-Va peninsula. Evolution 40:44–54.
ZAMUDIO, K. R., AND W. K. SAVAGE. 2003. Historical isolation, range expansion, and secondary contact of two highly divergent mitochondrial lineages in spotted salamanders (*Ambystoma maculatum*). Evolution 57:1631–1652.

Accepted: 17 February 2019.
Published online: 15 May 2019.

SUPPLEMENTARY DATA

Supplementary data associated with this article can be found online at http://dx.doi/10.1670/15-040.s1.

APPENDIX 1. Reagent volumes in cytochrome b PCR procedure. DNA concentrations were 50–100 ng/μL.

Reagent	Volume (μL)
5X Buffer	5
DNTPs	0.5
$MgCl_2$	1.5
Forward primer	1.25
Reverse primer	1.25
Taq polymerase	0.125
dH_2O	11.375
Template DNA	2

APPENDIX 2. Thermocycler protocol in cytochrome b PCR procedure. DNA concentrations were 50–100 ng/μL.

Step	Time (min:sec)	Temperature (°C)
1. Initialization	3:00	94
2. Denaturation	0:30	94
3. Annealing	1:00	53
4. Extension	1:15	72
5. Repeat steps 2–4 for 31 cycles		
6. Final extension	5:00	72

APPENDIX 3. Reagent volumes with Qiagen multiplex PCR kit in microsatellite PCR procedures for the three multiplex PCR reactions. Loci included in each multiplex are as follows: Multiplex 1: *Pc3, Pc28, Pc37*; Multiplex 2: *Pc7, Pc16, Pc 17*; Multiplex 3: *Pc15, Pc25, Pc30, Pc34* (Cameron et al., 2017). DNA concentrations were 50–100 ng/μL.

Reagent	Volume (μL)
2X PCR mix	12.81
10X primer mix	2.56
Qsol	2.56
dH_2O	6.24
Template DNA	1.5

APPENDIX 4. Thermocycler protocol in microsatellite PCR procedures for the three multiplex PCR reactions. Loci included in each multiplex are as follows: Multiplex 1: *Pc3, Pc28, Pc37*; Multiplex 2: *Pc7, Pc16, Pc 17*; Multiplex 3: *Pc15, Pc25, Pc30, Pc34* (Cameron et al., 2017). DNA concentrations were 50–100 ng/μL.

		Temperature (°C)		
Step	Time (min:sec)	Multiplex 1	Multiplex 2	Multiplex 3
1. Initialization	5:00	95	95	95
2. Denaturation	0:30	95	95	95
3. Annealing	1:30	60	60	56
4. Extension	0:30	72	72	72
5. Repeat steps 2–4 for 35 cycles				
6. Final extension	10:00	68	68	68

APPENDIX 5. Proportions of alleles in each population assigned by INTROGRESS to the first reference population, using site 1 (putatively OH clade; $n = 16$) and site 16 (putatively PA clade; $n = 14$) as the first and second reference populations, respectively. Results should be interpreted with caution because tests for population structure and hybrid identification indicate all populations, including reference populations, are within the same cluster, but do not indicate if this cluster corresponds with the OH or PA clade.

Site	PC3	PC37	PC28	PC7	PC17	PC16	PC30	PC25	PC34	PC15
1	0.0	0.0	0.0	0.7	0.9	0.4	0.0	0.8	0.2	1.0
2	0.0	0.0	0.0	0.8	0.7	0.5	0.0	0.9	0.0	0.8
3	0.0	0.0	0.0	0.9	0.9	0.6	0.0	0.7	0.1	0.8
4	0.0	0.0	0.0	0.6	0.6	0.4	0.0	0.3	0.1	0.8
5	0.0	0.0	0.0	0.8	0.7	0.3	0.0	0.5	0.1	0.9
6	0.0	0.0	0.0	0.5	0.7	0.3	0.0	0.7	0.1	0.9
7	0.0	0.0	0.0	0.8	0.9	0.4	0.0	0.5	0.3	0.8
8	0.0	0.0	0.0	1.0	0.9	0.4	0.0	0.7	0.1	0.9
9	0.0	0.0	0.0	0.5	1.0	0.6	0.0	0.8	0.0	0.9
10	0.0	0.0	0.0	0.7	0.8	0.5	0.0	0.7	0.2	0.7
11	0.0	0.0	0.0	0.9	0.9	0.5	0.0	0.5	0.0	1.0
12	0.0	0.0	0.0	0.9	0.8	0.3	0.0	0.9	0.1	0.8
13	0.0	0.0	0.0	1.0	0.8	0.3	0.0	0.5	0.0	0.9
14	0.0	0.0	0.0	0.9	0.7	0.6	0.0	0.8	0.1	0.6
15	0.0	0.0	0.0	0.8	0.9	0.4	0.0	0.9	0.2	0.9
16	0.0	0.0	0.0	0.9	0.9	0.7	0.0	0.7	0.0	0.8

Appendix 6

Cline-fitting procedure in HZAR 0.2-5 (Derryberry et al., 2014): To first reduce spatial coordinates of sampling localities to a one-dimensional coordinate system, we fit a regression line to projected coordinates of the points. Spatial coordinates (X, Y) were then converted into single coordinate values, χ, using $\chi = X\cos(\theta) + Y\cos(\theta)$, in which θ is the angle between the regression line (cline axis) and the east–west parallel (Rieux et al., 2013). Values were standardized so each point reflected the single-coordinate distance (km) from the westernmost site (1; $\chi = 0$ km). We conducted the analysis without scaling ($p_{\min} = 0$; $p_{\max} = 1$) because haplotype frequencies ranged from 0 to 1. We fit data to a simple, two-parameter cline model to estimate the cline center, c, and width (inverse of the maximum slope), w. We explored four additional models that assume tailed clines with two parameters, delta (δ, distance from cline center to the tail) and tau (τ, slope of the tail). These models were (1) right tail, (2) left tail, (3) mirrored left and right tails, and (4) independent left and right tails. We estimated covariance of parameters for each model with the use of MCMC analysis with a burn-in of 10^5 iterations followed by 10^6 iterations, sampling every 100 iterations (Derryberry et al., 2014). We ran three MCMC chains with the same number of iterations and burn in, and visually assessed runs for stationarity. We compared models to a null model that assumed no cline in the sampling region, and considered the model with the lowest AICc score the best-fit model. Two log-likelihood support units indicate the confidence interval around each estimated parameter.

Appendix 7

Summary statistics for microsatellite loci when individuals were grouped by mtDNA clade. Abbreviations indicate number of individuals (n), effective number of alleles (N_e), observed and expected heterozygosity (H_O and H_E), and the Weir and Cockerham (1984) inbreeding coefficient (F_{IS}).

MtDNA clade	Locus	n	No. of alleles	N_e	Private alleles	H_O	H_E	F_{IS}
OH	PC3	155	2	1.013	0	0.013	0.013	−0.003
	PC37	155	3	1.026	1	0.013	0.026	0.497
	PC28	155	5	1.147	1	0.123	0.128	0.048
	PC7	156	6	2.226	2	0.481	0.551	0.130
	PC17	157	6	1.983	0	0.433	0.496	0.130
	PC16	157	10	2.425	3	0.611	0.588	−0.037
	PC30	159	2	1.019	0	0.019	0.019	−0.006
	PC25	159	18	10.904	1	0.830	0.908	0.089
	PC34	159	3	1.269	0	0.189	0.212	0.113
	PC15	159	9	1.444	1	0.314	0.308	−0.019
PA	PC3	155	3	1.095	1	0.077	0.087	0.108
	PC37	155	3	1.020	1	0.019	0.019	−0.004
	PC28	155	6	1.351	2	0.284	0.260	−0.090
	PC7	156	4	1.875	0	0.346	0.467	0.261
	PC17	155	7	2.513	1	0.606	0.602	−0.004
	PC16	156	13	2.790	6	0.583	0.642	0.094
	PC30	157	3	1.052	1	0.051	0.050	−0.020
	PC25	156	20	7.300	3	0.769	0.863	0.112
	PC34	157	4	1.175	1	0.146	0.149	0.022
	PC15	157	13	1.683	5	0.420	0.406	−0.033